Numerical Modeling of Multi-Material Active Magnetic Regeneration

Nielsen, Kaspar Kirstein; Engelbrecht, Kurt; Bahl, Christian Robert Haffenden; Smith, Anders; Pryds, Nini; Hattel, Jesper Henri

Published in:
ExHFT-7

Publication date:
2009

Document Version
Publisher's PDF, also known as Version of record

ExHFT-7
28 June – 03 July 2009, Krakow, Poland

NUMERICAL MODELING OF MULTI-MATERIAL ACTIVE MAGNETIC REGENERATION

K.K. Nielsen[1,2,*], K. Engelbrecht[2], C.R.H Bahl[2], A. Smith[2], N. Pryds[2], J. Hattel[1]

[1]Department of Mechanical Engineering, Technical University of Denmark
Building 425, Niels Koppels Allé, DK-2800 Kgs. Lyngby, Denmark
[2]Fuel Cells and Solid State Chemistry Division
Risø National Laboratory for Sustainable Energy
Technical University of Denmark - DTU, Frederiksborgvej 399, DK-4000, Denmark

ABSTRACT. Magnetic refrigeration is a potentially environmentally-friendly alternative to vapour compression technology that is presented in this paper. The magnetocaloric effect in two magnetocaloric compounds in the $La(Fe,Co,Si)_{13}$ series is presented in terms of their adiabatic temperature change and the specific heat as a function of temperature at constant magnetic field. A 2.5-dimensional numerical model of an active magnetic regenerative (AMR) refrigerator device is presented. The experimental AMR located at Risø DTU has been equipped with a parallel-plate based regenerator made of the two materials. Experimental zero heat-load temperature spans are presented for different operating conditions and the results are compared to predictions of the numerical model. It is concluded that the model reproduces the experimental tendencies and when including thermal parasitic losses to ambient and the predictions from the model are within 1.5 K of the experimental results.

Keywords: active magnetic regeneration, numerical modeling, magnetocaloric effect

1. INTRODUCTION

1.1. Magnetic refrigeration and some of the challenges

Magnetic refrigeration is a research field covering a wide range of different physical disciplines. The basic physical property on which magnetic refrigeration is based is the magnetocaloric effect (MCE). This effect is exhibited by magnetic materials where increased ordering may be introduced by applying a magnetic field, thus lowering the magnetic entropy. This makes the MCE an inherently fundamental quantum mechanical effect. If the field is applied under adiabatic conditions the temperature of the material will rise. In order to maintain constant total entropy the decrease of the magnetic entropy must be compensated by an increase of the lattice and electron entropies thus increasing the temperature. This makes the MCE observable on the macroscopic level. The MCE is reversible for many magnetocaloric materials of interest but some materials exhibit some magnetic hysteresis [1].

For refrigeration applications the MCE can be used with the magnetocaloric material (MCM) as a refrigerant to accept a cooling load over a temperature span. However, the magnitude of the MCE is rather small – with an adiabatic temperature change with magnetization on the order a few K per tesla of magnetic flux density. This obviously limits the applicability of the MCE as a potential refrigerant.

* Corresponding author: K.K. Nielsen
Phone: + 45 4677 4758
E-mail address: kaki@risoe.dtu.dk

However, by implementing a regenerative, or active magnetic regeneration (AMR), cycle the technology can be used to absorb a cooling load at a temperature span that is higher than the adiabatic temperature change of the MCM. This process exploits the MCM in two ways; by using the MCE as work input to generate cooling and as a regenerator to store heat temporarily and build up a temperature gradient. This makes temperature spans larger than the adiabatic temperature change possible. The AMR process is composed of four sub processes. First the material is magnetized and thus the temperature in the solid regenerator rises. Second, a heat transfer fluid – typically water-based – is pushed through the material (which is designed in some porous configuration) from the cold to the hot end thus lowering the temperature of the material by rejecting heat to the ambient while still magnetized. The third step is demagnetization. This ensures the material to cool below the initial temperature. The fourth and final step is moving fluid towards the cold end, thus absorbing a heat load from the cooled space. Thus, magnetic refrigeration includes the fundamental MCE as well as macroscopic heat transfer and fluid dynamics.

The challenges are many within this area of research; issues like regenerator geometry (particle bed, parallel plates etc.), operating conditions (cycle frequency, fluid movement etc.) and the magnetocaloric properties of the MCM just to mention a few. The MCE is most pronounced over a relatively small temperature span around the Curie temperature (T_C) of the material (where a ferromagnetic material changes to its paramagnetic state). This limits the optimal operating temperature for any given MCM and thus constructing a regenerator of a series of materials each with its own working temperature range tuned to the local regenerator temperature experienced by each material can greatly increase the total MCE in the regenerator. This work is concerned with a first attempt to model an experimental setup with two materials configured in a parallel-plate stack of magnetocaloric plates of sintered La(Fe,Co,Si)13 made by Vacuumschmelze, Germany [2,3]. Using this material, experiments have been performed using the experimental AMR device located at Risø DTU, Technical University of Denmark. The device is a single regenerator reciprocating AMR that is discussed in more detail in [4] and [5]. Results of this and corresponding modeling results are the scope of this paper. Previous AMR modeling including comparisons with experimental results can be found in e.g. [6,7].

1.2. The magnetocaloric effect

The MCE is typically discussed in three different forms: The isothermal magnetic entropy change (ΔS_{mag}) when magnetizing a sample of a MCM, the adiabatic temperature change (ΔT_{ad}), i.e. the temperature change of a MCM when magnetized adiabatically and finally the specific heat capacity, c_H, as function of temperature, T, at constant magnetic field, H. The adiabatic temperature changes of two magnetocaloric materials are given in Figure 1. The materials are two different $La(Fe,Co,Si)_{13}$ compounds. The Fe/Co ratio has been varied in order to change the Curie temperature [2]. The figure shows the adiabatic temperature change when magnetizing from 0 T to 1.1 T. Some important details should be observed in the figure. Firstly, the clearly visible position of either material's transition temperature (in this case defined as the peak of the (ΔT_{ad}), curves). Secondly, the temperature ranges where each material exhibits a significant MCE overlap somewhat. Whether this overlap is sufficient for utilizing both materials in an effective refrigeration process is to be decided from modeling and experimental studies. In this paper we address some of these issues. It should be noted that the MCE for these materials is reversible. This is important since irreversibility associated with magnetization and demagnetization, known as magnetic hysteresis, is a serious degrading factor when considering the material's application as a refrigerant.

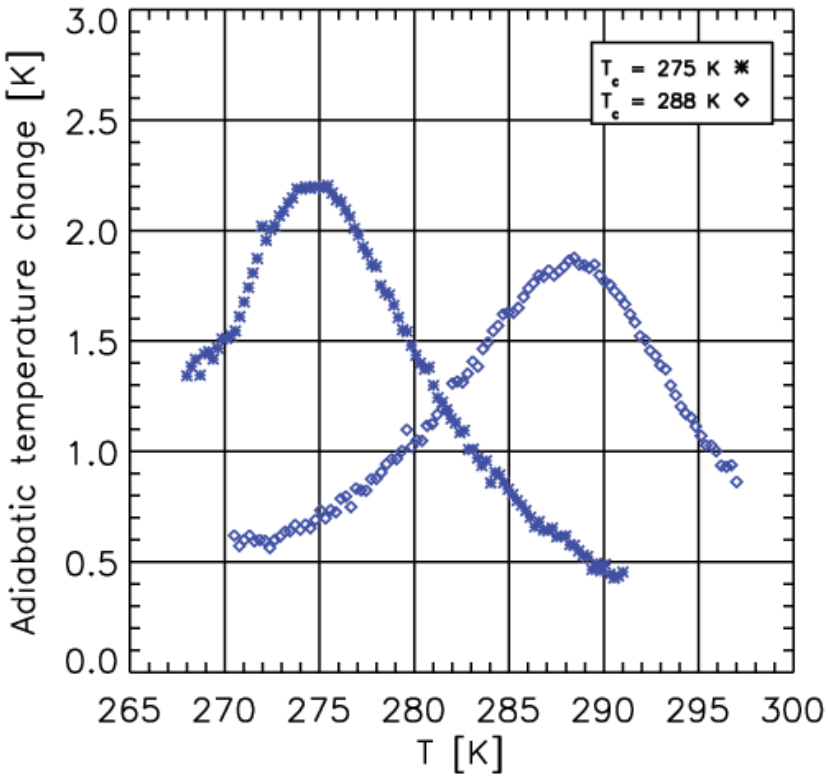

Figure 1: The adiabatic temperature change of two different compositions of $La(Fe,Co,Si)_{13}$ when magnetized from 0 to 1.1 Tesla. The indicated T_c in the figure legend is the Curie temperature of the materials.

The specific heat in an applied magnetic field has so far only been measured in detail on the compound with the low transition temperature and is given by [3]. Figure 2 shows the temperature dependence of the zero-field and the 1.0 T specific heat. Notice two important factors: First the peak value shifts significantly (3.5 K) between the two applied magnetic fields. Second, the zero-field specific heat has a higher and narrower peak than the 1.0 T specific heat curve has.

2. NUMERICAL AMR MODEL

The experimental device mentioned previously is modeled through a versatile 2.5-dimensional numerical model of a parallel plate AMR. The solution domains consist of a fluid domain and three solid domains; the MCM plate and a hot and cold heat exchanger (HEX). The governing equations are

$$\frac{\partial T_f}{\partial t} = \frac{k_f}{\rho_f c_{p,f}} \nabla^2 T_f + q_{bd,fc} + q_{bd,fh} + q_{bd,fMCM} + q_{loss,f} - u\frac{\partial T_f}{\partial x} \tag{1}$$

$$\frac{\partial T_{MCM}}{\partial t} = \frac{k_{MCM}}{\rho_{MCM} c_{H,MCM}} \nabla^2 T_{MCM} - q_{bd,fMCM} + q_{loss,MCM} \tag{2}$$

$$\frac{\partial T_c}{\partial t} = \frac{k_c}{\rho_c c_{p,c}} \nabla^2 T_c - q_{bd,fc} + q_{loss,c} \tag{3}$$

$$\frac{\partial T_h}{\partial t} = \frac{k_h}{\rho_h c_{p,h}} \nabla^2 T_h - q_{bd,fh} + q_{loss,h} \tag{4}$$

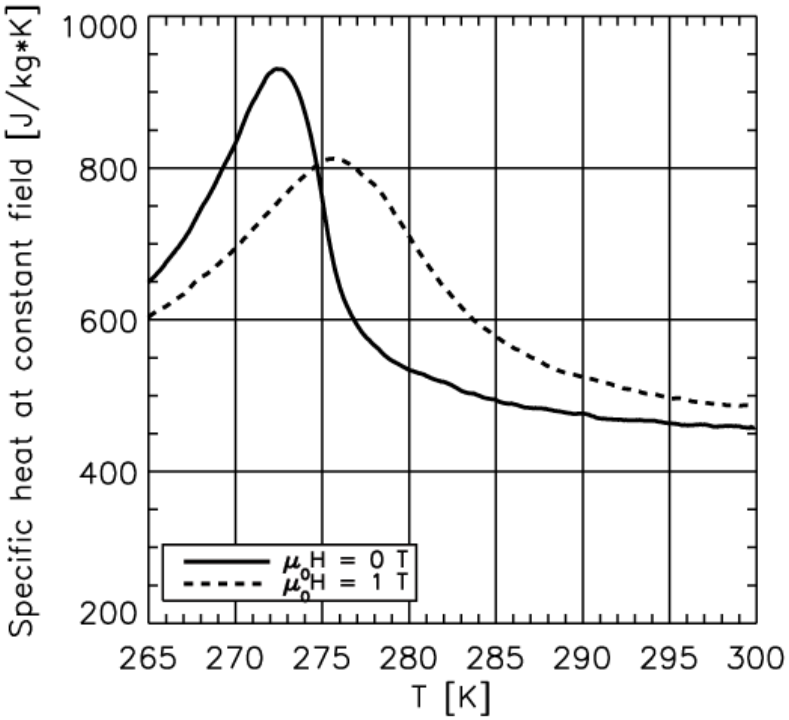

Figure 2: The specific heat capacity at constant magnetic field of the $La(Fe,Co,Si)_{13}$ sample with T_C = 275 K. Notice both the lower peak value as well as the lowering and broadening of the in-field specific heat.

The subscripts *f*, *MCM*, *c* and *h* indicate fluid, MCM, cold and hot HEX respectively. The thermal properties ρ and *k* denoting the mass density and the thermal conductivity have been introduced. The domains, as illustrated in Figure 3, are coupled via the boundary heat fluxes with subscripts *bd*.

The solution to Equations. (1)-(4) is determined for a number of cycles each divided in four sub processes further divided in time steps until cyclic steady-state is reached. The four sub-processes are: Magnetization (duration: τ_1 seconds), fluid flow from cold to hot end (hot blow, duration: τ_2 seconds), demagnetization (duration: τ_3 seconds) and finally flow from hot to cold end (cold blow, duration: τ_4 seconds). The cycle is assumed symmetric and thus $\tau_1 = \tau_3$ and $\tau_2 = \tau_4$. The numerical details can be found in [8]. The thermal properties used in the model are given in

Table 1.

Thermal parasitic losses to the ambient are enabled through the q_{loss} terms in Equations. (1)-(4). These are formulated on the form

$$q_{loss} = \frac{T - T_\infty}{\sum_i R_i}. \tag{5}$$

The ambient temperature is denoted by T_∞ and the thermal resistances R_l are to be summed over for each numerical grid cell. An example of such a summation is

$$R_{fl,total} = \frac{1/2\Delta z_f}{k_f \Delta x \Delta y} + \frac{\Delta z_{pl}}{k_{pl} \Delta x \Delta y} + \frac{1}{h_{conv} \Delta x \Delta y}, \tag{6}$$

which is representative for the fluid channel. Here $\Delta x, \Delta y$ and Δz denote the dimensions of the grid cell and h_{conv} the passive convective heat transfer coefficient modeling the heat loss on the outside of the regenerator to the ambient.

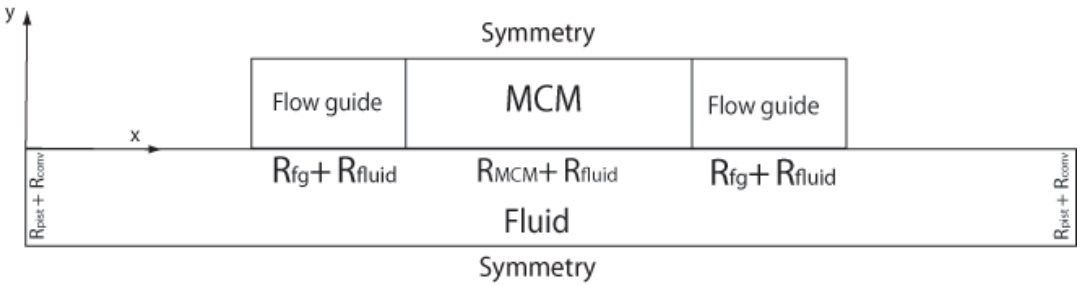

Figure 3: The four solution domains of the numerical AMR model. The domains denoted flow guide, are able to act as either passive plastic flow guides or as HEXs with perfect contact to the ambient (the hot HEX) or to a heat load (cold HEX). The symmetry lines indicate that only half a flow channel and half a solid domain are solved for. The indication of thermal resistances shows the internal thermal boundaries between the domains.

3. RESULTS

In the following results from both modeling and the experimental AMR device located at Risø DTU, are presented. The MCE was modeled discretely in the sense that at the first timestep of the AMR cycle the adiabatic temperature change from magnetizing was applied. Similarly, halfway through the modeled cycle (at the end of the hot blow) the adiabatic temperature change from demagnetizing was applied in one timestep. The specific heat was applied similarly. Here the data set from the 1.0 T measurements was used to temperature-interpolate the specific heat in the first half of the AMR cycle. In the last half of the cycle the zero-field specific-heat table was used. The adiabatic temperature change data is as previously shown in Figure 1. The specific heat is shown in Figure 2. However, since the specific heat of the high transition temperature material is not yet available, the specific heat data of the low-transition temperature material was used but shifted 13 K higher on the temperature scale (matching the difference between the peak values in the adiabatic temperature change values, see Figure 1).

The experimental approach is described thoroughly in both [4,5]. The range of the operating parameters are given in

Table 2. Both experiments were performed with a regenerator using the two materials (each 20 mm long yielding in total a 40 mm long regenerator). The flow channel height was 0.5 mm and the thickness of the plates 0.9 mm. All experiments were performed at an ambient temperature, T_∞, approximately equal to 287 K, which was also used as the input ambient temperature to the model. A total of 11 plates were used.

The model is able to simulate thermal parasitic losses to the ambient modeled via thermal resistances as described in Equations. (5)-(6). Modeling both with and without this loss has been performed. The results from the two experimental situations are given in Figure 4 and Figure 5. Here it is clearly seen that including the thermal parasitic losses improves the model's ability to reproduce the experimental results.

Table 1
Thermal properties of the computational domains. Data for copper is used for the HEXs. The thermal conductivity of the MCM was estimated from the results of [9,10].

	ρ [kg/m^3]	c [J/kg·K]	k [W/m·K]
Fluid	1000	4200	0.6
MCM	7100	500-950	9
HEXs	8933	385	401
Housing	N/A	N/A	0.2

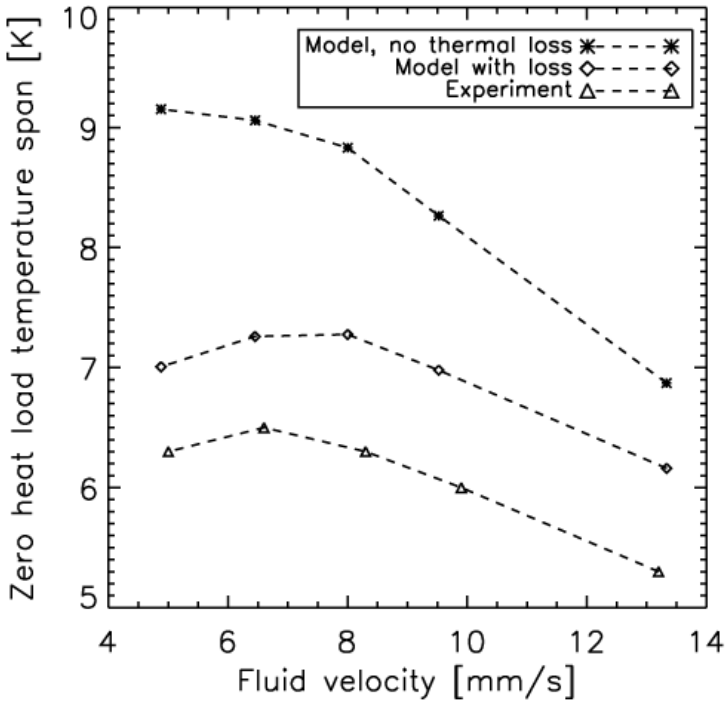

Figure 4: The no heat-load temperature span of experiment #1 (see Table 2 for details).

Overall, the predictions of the thermal loss model overestimate no more than 1.5 K in the worst case and in general about only 1 K, compared to the experimental results. The motivation for performing the two sets of experiments was to change the utilization defined as:

$$U = \frac{\rho_{fl} c_{p,fl} H_{fl} \Delta x}{\rho_{MCM} c_{H,MCM} H_{MCM} L_{MCM}}. \quad (7)$$

Where ρ_{fl} is the mass density of the heat transfer fluid, $c_{H,fl}$ is the specific heat of the fluid, H_{fl} is the thickness of the fluid channel, Δx is the stroke length, ρ_{MCM} is the mass density of the MCM, H_{MCM} is the thickness of the MCM plate, $c_{H,MCM}$ is the mean specific heat of the MCM, and L_{MCM} is the length of the MCM plate. Thus, the utilization expresses the fraction of thermal mass of fluid moved compared to the thermal mass of the MCM. The mean specific heat of the MCM was set to 550 J/kgK. Now, the two values of the utilization (which characterize the two experiments respectively) are kept constant by varying the fluid velocity and the timing of the AMR cycle. Thus, a low fluid velocity means a higher cycle time. Therefore, the fact that the model reproduces the experiment at low fluid velocities closer than at high is explained by the fact that thermal losses affect performance more in a slow cycle than a faster cycle. Also, the largest temperature span, and thus the highest conduction loss to the surroundings, is achieved with a relatively slow fluid velocity (not the slowest – the temperature span curves clearly have a peak fluid velocity).

Table 2
The operating parameters of the two experiments.

Experiment	Utilization [-]	Timing range [s]	Fluid velocity range [mm/s]
#1	0.51	5 s – 10.2 s	5.0 – 13.3
#2	0.81	7 s – 15.4 s	5.0 – 13.3

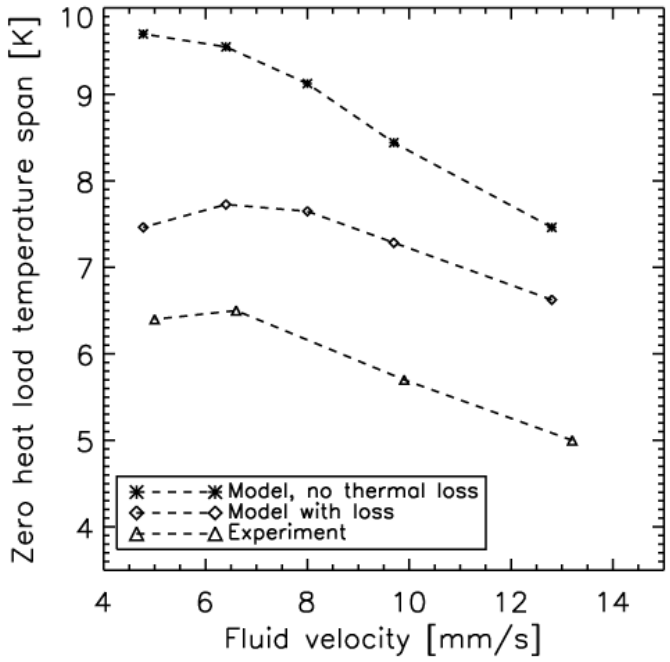

Figure 5: no heat-load temperature span of experiment #2 (see Table 2 for details).

4. DISCUSSION AND CONCLUSION

The comparison between experimental results and modeling of the experiment shows that the numerical AMR model presented here is able to reproduce the tendencies of the experiment. When including thermal losses to the ambient it is furthermore seen that the model results improve significantly in reproducing the experimental values. However, a discrepancy still exists. This may partially be explained by the use of the specific heat of the low-transition temperature material as the specific heat of the high-transition temperature material. Also the internal magnetic field in the MCM is somewhat reduced compared to the external field due to demagnetization [11]. Furthermore, the regenerator is comprised of 11 plates of MCM and will be subject to variation in thermal losses and spatially varying magnetic flux densities, which is not included by the model since the modelled geometry consists only of half a fluid channel and half a solid domain. Future work will include further modeling of the two-material regenerator in order to optimize for future choices of the transition temperatures of each individual material. As the maximum experimentally reached temperature span was about 6.5 K and the ambient was at 287 K the low-transition temperature material was clearly not as active as it could be and was thus not utilized fully.

ACKNOWLEGEMENT

We thank Mr. Jørgen Geyti for his technical help. Also, we thank Vacuumschmelze GmbH & Co. KG, 63450 Hanau, Germany for supplying the plates of $La(Fe,Co,Si)_{13}$. The authors further acknowledge the support of the Programme Commission on Energy and Environment (EnMi) (Contract No. 2104-06-0032), which is part of the Danish Council for Strategic Research.

REFERENCES

1. Gschneidner, K. A., V. K. Pecharsky, and A. O. Tsokol. "Recent Developments in Magnetocaloric Materials." *Rep. Prog. Phys.* 68 (2005):1479-1539.

2. Katter M., V. Zellmann, G.W. Reppel, and K. Uestuener. "Magnetocaloric properties of $La(Fe,Co,Si)_{13}$ bulk material prepared by Powder Metallurgy", *IEEE Trans. Magn.* 44 (2008) 3044.

3. Hansen, B. R., M. Katter, L. Theil Kuhn, C. R. H., A. Smith, and C. Ancona-Torres. "Characterization study of a plate of the magnetocaloric material La(Fe,Co,Si)13." 2009. *Proc. 3rd International Conference on Magnetic Refrigeration at Room Temperature, IIF/IIR.*

4. Bahl, C.R.H., T.F. Petersen, N. Pryds, and A. Smith. "A versatile magnetic refrigeration test device." *Review of Scientific Instruments* 79 (2008): 093906.

5. Engelbrecht, K., J. B. Jensen, C. R. H., and N. Pryds. "Experiments on a modular magnetic Refrigeration Device." 2009. *Proc. 3rd International Conference on Magnetic Refrigeration at Room Temperature, IIF/IIR.*

6. Dikeos, J., A. Rowe, and A. Tura. "Numerical Analysis of an Active Magnetic Regenerator (AMR) Refrigeration Cycle." *AIP Conference Proceedings* 823 (2006): 993-1000.

7. Engelbrecht, K.L., G.F. Nellis, S.A. Klein, and A.M. Boeder. "Modeling active magnetic regenerative refrigeration systems." Refrigeration Science and Technology Proceedings, 2005. 265-274.

8. Nielsen, K.K., R. Bjørk, C.R.H. Bahl, N. Pryds, A. Smith, and J. Hattel. "Detailed numerical modeling of a linear parallel-plate Active Magnetic Regenerator." *Accepted for publication in the International Journal of Refrigeration*, 2009.

9. Fujieda, S., Y. Hasegawa, A. Fujita, and K. Fukamichi. "Thermal transport properties of magnetic refrigerants La(Fex Si1-x)13 and their hydrides, and Gd5 Si2Ge2 and MnAs." *Journal of Applied Physics* (AIP, USA) 95 (2004): 2429-2431.

10. Fukamichi, K., A. Fujita, and S. Fujieda. "Large magnetocaloric effects and thermal transport properties of La(FeSi)13 and their hydrides." *Journal of Alloys and Compounds* (Elsevier, Switzerland) 408-412 (2006): 307-12.

11. Bahl, C.R.H., and K.K. Nielsen. "The effect of demagnetization on the magnetocaloric properties of gadolinium." *Journal of Applied Physics* 105 (2009): 13916.